ATOM Core Startup Simulation with 3-D TH-Coupled Quasi-Static Nodal Method

Yunseok Jeong, Ahmed Amin E. Abdelhameed, and Yonghee Kim*
Korea Advanced Institute of Science and Technology (KAIST)
291 Daehak-ro, Yuseong-gu, Daejeon, Korea, 34141
yongheekim@kaist.ac.kr

1. Introduction

The water-cooled small modular reactor (SMR) has been considered as one of the next generation nuclear reactor concepts due to its enhanced passive safety and advanced design concepts [1].

Soluble-boron is actively used in commercial PWRs because it does not distort local power distribution and most SMRs are using the soluble boron for reactivity control. However, it has several drawbacks such as slow reactivity response, near-zero moderator temperature coefficient (MTC) issue with a high soluble-boron concentration, etc. [2,3]. With those issues, the existence of soluble-boron obstructs flexible load-following operations of SMRs. Meanwhile, it was studied and demonstrated that a soluble-boron-free (SBF) reactor design has advantages for passively autonomous load-follow and frequency control operations [4,5].

To overcome those drawbacks and take advantage of merits of SMR, a soluble-boron-free SMR design with a small excess reactivity at beginning of cycle was introduced. This was named the ATOM (Autonomous transportable on-demand reactor module) [6]. It contains Gd_2O_3-based centrally-shielded burnable absorbers (CSBA). Due to the presence of CSBAs, the ATOM core can achieve a very small burnup reactivity swing without soluble-boron.

Since the ATOM core only uses control rods for reactivity control, the startup process including power ascension must be investigated and optimized to reach hot full power while supervising Xe-135 concentration, ASI, fuel and coolant temperature, etc. Previously, the startup from a cold zero power to hot zero power for an SBF system was preliminarily performed in 2016 [7], but hot zero power startup was not investigated yet.

In this paper, the ATOM core startup simulation from hot zero power (HZP) to hot full power (HFP) was performed by using an in-house three-dimensional thermal-hydraulics coupled reactor analysis code with a quasi-static method to test successful completion of the startup.

2. Neutronics Modeling

The two-step analysis was used to calculate reactor parameters because the ATOM core is a light-water reactor. The burnup-dependent cross sections, temperature sensitivities, ADFs were calculated by using Serpent-2 3-D Monte Carlo simulations with the ENDF/B-VII.1 cross-section library. The burnup- and temperature-dependent cross sections were calculated with Eq. (1) in this work.

$$\Sigma_a(Bu, T_f, T_m, D_m)$$
$$= \Sigma_a^{ref}(Bu) + \frac{\partial \Sigma_a}{\partial \sqrt{T_f}} \Delta \sqrt{T_f} + \frac{\partial \Sigma_a}{\partial T_m} \Delta T_m$$
$$+ \frac{\partial \Sigma_a}{\partial D_m} \Delta D_m + \frac{1}{2} \frac{\partial^2 \Sigma_a}{\partial D_m^2} (\Delta D_m)^2 \qquad (1)$$
$$+ N_{Hom}^{Xe,\infty}(\phi_g) \sigma_a^{Xe}(Bu, T_f, T_m, D_m)$$
$$+ N_{Hom}^{Sm,\infty}(\phi_g) \sigma_a^{Sm}(Bu, T_f, T_m, D_m)$$

Then 3-D nodal analysis was performed with a time-dependent FORTRAN-95 code, which solves TH-coupled reactor 2-group diffusion equations. The reactor core analysis with given conditions can be solved with nodal expansion method (NEM) or semi analytical nodal method (SANM) [8].

The steam generator was decoupled and the coolant inlet temperature was determined by power demand with constant average coolant temperature strategy, which was adopted in the ATOM system because the reactivity change can be minimized during a power transient.

Since the startup simulation needs the control rod criticality search, the quasi-static (QS) method was used for reactor core analysis to reduce computing time at every one hour, which is one fourth of each power ramping interval. However, Xe-135 and Sm-149 concentrations were calculated in time-dependent method with Eqs. (2)-(5).

$$N_I(t_n + \Delta t) = N_I(t_n) \qquad (2)$$
$$+ \Delta t(\gamma_I \sum_{g=1}^{G} \Sigma_{f,g}(t_n)\phi_g(t_n) - \lambda_I N_I(t_n))$$

$$N_{Xe}(t_n + \Delta t) = N_{Xe}(t_n) + \Delta t(\lambda_I N_I(t_n) + \gamma_{Xe} \sum_{g=1}^{G} \Sigma_{f,g}(t_n)\phi_g(t_n) \qquad (3)$$
$$- \lambda_{Xe} N_{Xe}(t_n) - \sum_{g=1}^{G} \sigma_{Xe,a,g}(t_n)N_{Xe}(t_n)\phi_g(t_n))$$

$$N_{Pm}(t_n + \Delta t) = N_{Pm}(t_n) \qquad (4)$$
$$+ \Delta t(\gamma_{Pm} \sum_{g=1}^{G} \Sigma_{f,g}(t_n)\phi_g(t_n) - \lambda_{Pm} N_{Pm}(t_n))$$

$$N_{Sm}(t_n + \Delta t) = N_{Sm}(t_n) + \Delta t(\lambda_{Pm} N_{Pm}(t_n) \qquad (5)$$
$$- \sum_{g=1}^{G} \sigma_{Sm,a,g}(t_n)N_{Sm}(t_n)\phi_g(t_n))$$

To mimic real startup situation from HZP, the initial control rod positions were properly set in the numerical simulations: the shutdown bank is all fully withdrawn,

and all regulating banks and mechanical shim banks are fully inserted.

The criticality search was performed after every QS calculation until it finds control rod critical height with an error of 10pcm. The moving CEAs were selected with pre-determined withdrawal priority.

3. Thermal-Hydraulic (TH) Modeling

The thermal-hydraulic analysis was done for all fuel assemblies in the ATOM core. From the reactor analysis information, axial temperature distributions can be calculated with the coolant inlet temperature obtained from power demand.

First, the axial pressure drop which satisfies the mass balance equation is found from axial momentum balance equation and coolant flow velocity and pressure drop are updated until the mass balance is satisfied. Then, the energy balance equation is solved until the convergence of enthalpy and coolant temperature. In this TH model, the lateral momentum was not included and axial heat conduction was ignored. Therefore, all fuel pin sub-channels have identical TH parameters and all terms related with the lateral momentum are neglected. Eqs. (6)-(8) are mass balance equation, axial momentum equation, and energy balance equation used in TH analysis respectively [9].

$$(\dot{m}_i - \dot{m}_{i-1}) = -\Delta z_i A_i \frac{\partial \rho_i}{\partial t} \tag{6}$$

$$\frac{(\dot{m}_i v_i - \dot{m}_{i-1} v_{i-1})}{\Delta z_i} + \frac{\partial \dot{m}_i}{\partial t} = -A_i \rho_i g - A_i \frac{\Delta P_i}{\Delta z_i} - \frac{F_i}{\Delta z_i} \tag{7}$$

$$A_i \frac{\partial (\rho_i h_i)}{\partial t} + \frac{(\dot{m}_i h_i - \dot{m}_{i-1} h_{i-1})}{\Delta z_i} = q_i' \tag{8}$$

where,

$$F_i = \frac{1}{2}\left(f \frac{\Delta z \phi^2}{D_h \rho_i} + KV^* \right)_i \frac{|\dot{m}_i|\dot{m}_i}{A_i},$$

$$f = a\mathrm{Re}^b, \begin{cases} a = 0.32, b = -0.25 \text{ for larminar} \\ a = 64, b = -1 \text{ for turbulent} \end{cases} \tag{9}$$

$$\mathrm{Re} = \frac{\rho v D_h}{\mu}, \quad D_h = d\left(\frac{4(p/d)^2}{\pi} - 1 \right)$$

The index i stands for axial node level for each assembly channel. $\dot{m}_i$ and v_i are mass flow rate and speed of the coolant at i-th axial node, respectively. Δz_i is axial length of each axial node. q_i' is linear power density of each fuel assembly and h_i stands for the enthalpy of the coolant at axial node i.

In Eq. (7), F_i represents forces from wall friction and form drag. By using Eq. (9), it is calculated with friction factor f, unity phase multiplier ϕ, pressure loss coefficient of grid spacers K, specific volume V^*, and equivalent diameter D_h. In equivalent diameter, p and d are pitch and fuel pin diameter, respectively.

From the converged axial coolant temperature distribution, the temperature distribution from cladding surface to fuel center is calculated by using finite-difference method (FDM). Eq. (10) briefly describes the system matrix of heat conduction at fuel and cladding region. The method to construct the system matrix is similar with COBRA-III [10]

$$\rho_j C_p V_j \frac{\partial T_j}{\partial t} = Q_j'' V_j + Q_{j-1,j} + Q_{j+1,j}$$

$$Q_{i,j} = K_{i,j} \left[T_i - T_j \right],$$

$$K_{i,j} = \frac{2\pi r_i \Delta z (k_i k_j)}{k_j (r_i - \overline{r}_i) + k_i (\overline{r}_j - r_i)}, \tag{10}$$

$$\overline{r}_j = \frac{2(r_j^2 + r_j r_{j-1} + r_{j-1}^2)}{3(r_j + r_{j-1})}.$$

where,

$$C_p(T) = \frac{302.27(\theta/T)^2 e^{\theta/T}}{(e^{\theta/T} - 1)^2} + 2 \times 8.463 \times 10^{-3} T$$
$$+ 8.741 \times 10^7 E_a \frac{e^{-E_a/T}}{T^2}, \tag{11}$$

$$T_{fuel,eff} = \frac{23}{25} T_{fuel,average} + \frac{2}{25} T_{fuel,surface} \tag{12}$$

$$k_{fuel} = 1.05 + \frac{2150}{T_{eff} - 73.15}, \tag{13}$$

$$k_{cladding} = 7.51 + 2.09 \times 10^{-2} T_{cl} - 1.45 \times 10^{-5} T_{cl}^2$$
$$+ 7.67 \times 10^{-9} T_{cl}^3 \tag{14}$$

With Eq. (11), specific heat capacity of coolant was calculated. Here, θ is Einstein temperature and E_a is the electron activation energy divided by Boltzmann constant [11,12]. The effective fuel temperature for fuel temperature coefficient was calculated with Eq. (12) [13,14]. Then, thermal conductivities of UO_2 fuel and Zircaloy cladding were evaluated with Eqs. (13)-(14) [15]. A non-linear iteration was performed until the convergence of temperature since all TH parameters are temperature-dependent.

4. Numerical Results

In the numerical simulations, the beginning of cycle (BOC) condition was applied to initial power condition with Xe equilibrium state. In the initial condition, Sm-149 density was assumed to be zero since Sm-149 requires almost infinite time to reach an equilibrium at zero power. Also, the shutdown bank was fully withdrawn before the transient to make the ATOM core hot zero power (0.001%). Every regulating bank height was 15cm from the bottom of active core to find initial criticality height earlier. The pattern of mechanical shim banks and regulating banks are shown in Figure 1 [8].
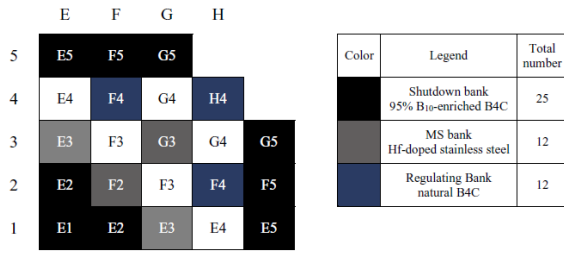
Figure 1. Control Rod Pattern

As seen in Figure 2, the power demand reached full power after 66 hours and total simulation time was 144 hours. The power ramp-up scenarios was step-increasing to mimic real startup. After reaching 100% power demand, it remained constant until the end of simulation.
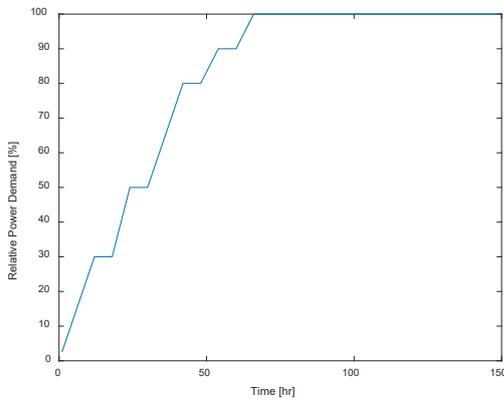
Figure 2. Power Demand

In Figure 3, Xe-135 concentration keeps increasing after reaching full power because of its long half-life comparing with transient speed. Xe-135 convergence was observed a few days after transient in this figure. However, Sm-149 concentration did not reach the convergence since the simulation is quite short when comparing with speed of Sm-149 accumulation and ATOM core has lower power density than commercial PWRs, which results in slow accumulation of the Xe and Sm negative reactivity.

Meanwhile, from Figure 4, the withdrawal of all regulating banks (F4, H4) started with increasing power demand. Because the simulation was performed with quasi-static method, the first point of control rod height in Figure 4 was about 36cm. Due to the negative reactivity of Xe-135 and Sm-149, the regulating bank withdrawal continued after reaching 100% power.

The ASI value is initially very high because the height of all regulating banks was almost at the middle of active core, which leads to highly bottom-skewed axial power shape. With increasing power demand, the regulating banks are continuously withdrawn and the ASI value showed decreasing trend. However, the ASI value is still quite high because of very slow convergence rate of Sm-149. With Eq. (5) and hot full

power flux of ATOM core, it requires about one month for convergence.
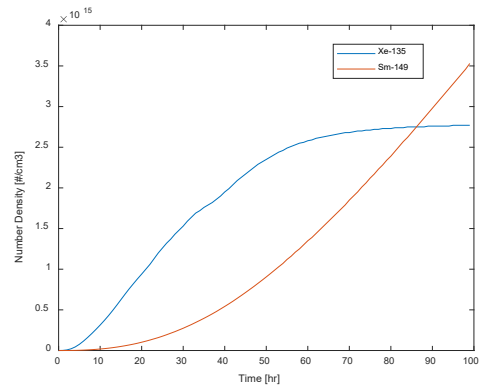
Figure 3. Xe-135, Sm-149 Concentration
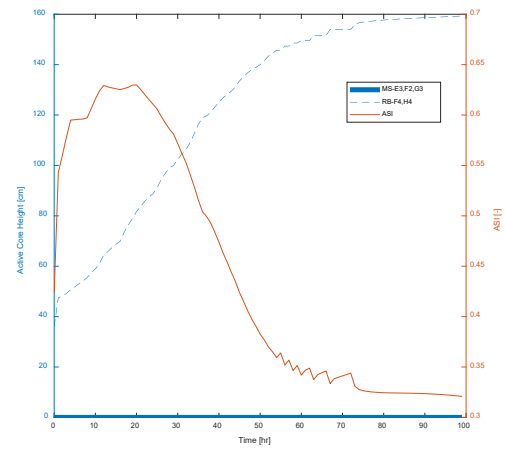
Figure 4. Critical Heights of the various CEAs and ASI

Both effective fuel temperature and coolant temperature are averaged over the whole fuel assemblies in the ATOM core. In Figure 5, since the inlet coolant temperature control strategy was constant average coolant temperature, inlet coolant temperature was controlled with power demand. Moreover, in Figure 6, the effective fuel temperature also increased with power demand. At each constant power demand interval, it slightly decreased by a maximum of 0.9K. The reason is that the accumulation of poisons provides negative reactivity and it slightly changed local power distribution even with identical power demand. Also, Figure 7 shows radial and 3D power peaking factors, which are near 1.2 and 1.8 at the end of the simulation, respectively. The 3D peaking factor is expected to decrease more after accumulation of Sm-149.
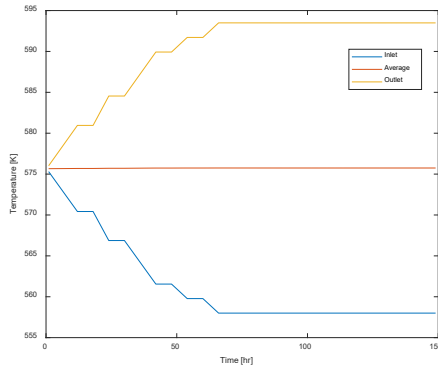
Figure 5. Coolant Temperature
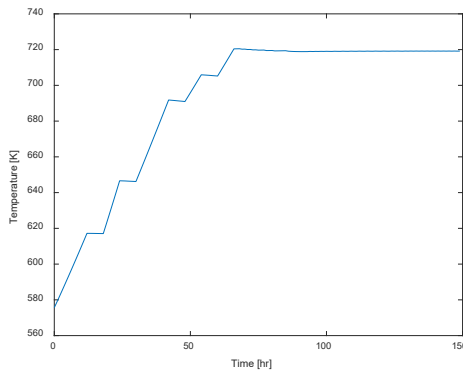
Figure 6. Effective Fuel Temperature
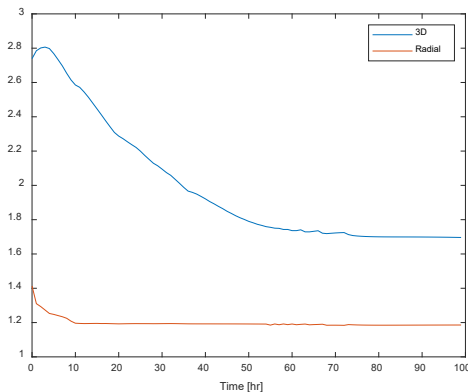
Figure 7. Power Peaking Factor

5. Summary and Conclusions

The ATOM core analysis for reactor startup from hot zero power to hot full power with 3-D TH-coupled quasi-static nodal method was performed to check the feasibility of reactor startup using control rods only. The total transient time was 100 hours to observe Xe-135 convergence behavior. It was demonstrated that the SBF ATOM reactor startup can be done by using control rods without violating core design criteria. For further studies, an advanced control rod selection module will be investigated to minimize the ASI change during the startup stage. Also, DNBR analysis with in-house code will be performed to optimize power ramp-up rate.

ACKNOWLEDGEMENTS

REFERENCES

[1] D.T. Ingersoll, and M.D. Carelli, eds. *Handbook of small modular nuclear reactors*. Elsevier, 2014.

[2] EPRI, Elimination of Soluble Boron for a New PWR Design, 1989 report document EPRI-NP-6536.

[3] M.S. Yahya, H. Yu, and Y. Kim. "Burnable absorber-integrated Guide Thimble (BigT)–I: design concepts and neutronic characterization on the fuel assembly benchmarks." *Journal of Nuclear Science and Technology* 53.7 (2016): 1048-1060.

[4] A.A.E. Abdelhameed, Haseeb ur Rehman, Y. Kim. "A Physics Study for Passively-Autonomous Daily Load-Follow Operation in Soluble-Boron-Free SMR." *ICAPP 2017*. ANS, 2017.

[5] A.A.E. Abdelhameed, Nguyen, X.H, Y. Kim, Feasibility of passive autonomous frequency control operation in a Soluble-Boron-Free small PWR, Ann. Nucl. Energy 116 (2018) 319-333.

[6] X.H. Nguyen, C. Kim, and Y. Kim. "An advanced core design for a soluble-boron-free small modular reactor ATOM with centrally-shielded burnable absorber." *Nuclear Engineering and Technology* 51.2 (2019): 369-376.

[7] A.A.E. Abdelhameed, M.S. Yahya, and Y. Kim. "Feasibility of Cold Nuclear Startup in Autonomous Soluble-Boron-Free SMR." In *Transactions of the Korean Nuclear Society Autumn Meeting, Gyeongju, Korea*.

[8] J. Yoon, H. Joo, 2008. Two-level coarse mesh finite difference formulation with multigroup source expansion nodal kernels. J. Nucl. Sci. Technol. 45 (7), 668-682.

[9] K.S. Chaudri, J. Kim, and Y. Kim. "Development and validation of a fast sub-channel code for LWR multi-physics analyses." *Nuclear Engineering and Technology* 51.5 (2019): 1218-1230.

[10] D. Basile, et al. "COBRA-EN: an upgraded version of the COBRA-3C/MIT code for thermal hydraulic transient analysis of light water reactor fuel assemblies and cores." *Radiation Safety Information Computational Center, Oak Ridge National Lab* (1999).

[11] S. G. Popov, J. J. Carbajo, V. K. Ivanov, and G. L. Yoder. "Thermophysical properties of MOX and UO_2 fuels including the effects of irradiation." *ORNL* 27 (2000): 4-00.

[12] J.K. Fink, T. Sofu, and H. Ley. "International nuclear safety center database on thermophysical properties of reactor materials." *International journal of thermophysics* 20.1 (1999): 279-287.

[13] G. Grandi, et al. "Effect of CASMO-5 cross-section data and Doppler temperature definitions on LWR reactivity initiated accidents." *Advances in Reactor Physics to Power the Nuclear Renaissance (PHYSOR 2010)* (2010).

[14] D. Tomatis. "Heat conduction in nuclear fuel by the Kirchhoff transformation." *Annals of Nuclear Energy* 57 (2013): 100-105.

[15] B. Cho, S. Yuk, N. Z. Cho, and Y. Kim. "User's manual for the rectangular three-dimensional diffusion nodal code COREDAX-2 version 1.8." *Korea Advanced Institute of Science and Technology (Aug. 2014)* (2016).